Paleoceanography and Paleoclimatology

RESEARCH ARTICLE
10.1029/2021PA004252

Special Section:
Cenozoic Evolution of Mountains, Monsoons, and the Biosphere

Enhanced Late Miocene Chemical Weathering and Altered Precipitation Patterns in the Watersheds of the Bay of Bengal Recorded by Detrital Clay Radiogenic Isotopes

Lisa Bretschneider[1], Ed C. Hathorne[1], Clara T. Bolton[2], Daniel Gebregiorgis[3], Liviu Giosan[4], Emmeline Gray[2,5], Huang Huang[1,6], Ann Holbourn[7], Wolfgang Kuhnt[7], and Martin Frank[1]

[1]GEOMAR Helmholtz Centre for Ocean Research Kiel, Kiel, Germany, [2]Aix Marseille Univ, CNRS, IRD, INRAE, Coll France, CEREGE, Aix-en-Provence, France, [3]Department of Geosciences, Georgia State University, Atlanta, GA, USA, [4]Woods Hole Oceanographic Institution, Falmouth, MA, USA, [5]The Open University, Milton Keynes, UK, [6]Sun Yat-Sen University, Guangzhou, China, [7]Institute of Geosciences, Christian-Albrechts-University Kiel, Kiel, Germany

Highlights:

- Radiogenic isotope compositions of detrital clays from the Bay of Bengal indicate a generally stable provenance from 9 to 5 Ma
- A step change in Nd and Pb isotope compositions at ~7.3 Ma reflects a climatically driven eastward shift in precipitation patterns resulting in enhanced erosion of the Indo-Burman Ranges
- Elevated $^{87}Sr/^{86}Sr$ between 6 and 5 Ma was likely related to increased chemical weathering caused by thicker soils and by C4 plant expansion

Supporting Information:

Supporting Information may be found in the online version of this article.

Correspondence to:

E. C. Hathorne,
ehathorne@geomar.de

Citation:

Bretschneider, L., Hathorne, E. C., Bolton, C. T., Gebregiorgis, D., Giosan, L., Gray, E., et al. (2021). Enhanced late Miocene chemical weathering and altered precipitation patterns in the watersheds of the Bay of Bengal recorded by detrital clay radiogenic isotopes. *Paleoceanography and Paleoclimatology*, *36*, e2021PA004252. https://doi.org/10.1029/2021PA004252

Received 5 FEB 2021
Accepted 8 AUG 2021

Abstract The late Miocene was a period of declining CO_2 levels and extensive environmental changes, which likely had a large impact on monsoon strength as well as on the weathering and erosion intensity in the South Asian Monsoon domain. To improve our understanding of these feedback systems, detrital clays from the southern Bay of Bengal (International Ocean Discovery Program Site U1443) were analyzed for the radiogenic isotope compositions of Sr, Nd, and Pb to reconstruct changes in sediment provenance and weathering regime related to South Asian Monsoon rainfall from 9 to 5 Ma. The 100 kyr resolution late Miocene to earliest Pliocene record suggests overall low variability in the provenance of clays deposited on the Ninetyeast Ridge. However, at 7.3 Ma, Nd and Pb isotope compositions indicate a switch to an increased relative contribution from the Irrawaddy River (by ~10%). This shift occurred during the global benthic $\delta^{13}C$ decline, and we suggest that global cooling and increasing aridity resulted in an eastward shift of precipitation patterns leading to a more focused erosion of the Indo-Burman Ranges. Sr isotope compositions were decoupled from Nd and Pb isotope signatures and became more radiogenic between 6 and 5 Ma. Grassland expansion generating thick, easily weatherable soils may have led to an environment supporting intense chemical weathering, which is likely responsible for the elevated detrital clay $^{87}Sr/^{86}Sr$ ratios during this time. This change in Sr isotope signatures may also have contributed to the late Miocene increase of the global seawater Sr isotope composition.

Plain Language Summary The South Asian or Indian monsoon affects the lives of billions. Through the erosion and weathering of rocks, the monsoon also has the potential to remove carbon dioxide from the atmosphere through increased weathering in the region including the Himalaya Mountains. The late Miocene, between 9 and 5 million years ago, was a period of global cooling and proliferation of grasslands in different regions including South Asia. Here, we examine the composition of clays formed by rock weathering during the late Miocene to determine their source region around the Bay of Bengal. The results suggest a generally stable mixture of sources with the strongest sources being regions with the highest monsoon rainfall today. We identify slight changes in the mixture of sources, which accompany a global change in carbon cycling, highlighting the role monsoon climate likely played in these changes. Toward the end of the Miocene, we identify a change in the Sr isotopes, which was not caused by source changes but by the strength of the rock weathering. This change has been observed in global records and it seems likely that it was driven by rock weathering in the South Asian Monsoon region.

1. Introduction

The late Miocene was an important period within the global Cenozoic cooling trend and was marked by extensive changes in marine and terrestrial environments and ecosystems (e.g., Cerling et al., 1997; Dupont et al., 2013; Herbert et al., 2016). This time interval was characterized by relative global warmth (Herbert et al., 2016; Westerhold et al., 2020; Zachos et al., 2008) and thus holds great potential to better understand

climate-carbon cycle dynamics on a warmer-than-modern Earth (Burke et al., 2018; Holbourn et al., 2018). Records of South Asian monsoon strength, erosion, and weathering in the late Miocene exist for the distal Indus and Bengal fans (e.g., Clift et al., 2008; Feakins et al.. 2020; Galy et al., 2010), but continuous and relatively high temporal resolution records are lacking.

As global climate cooled during the Miocene, the first ephemeral northern hemisphere glaciations occurred between 6 and 5.5 Ma (DeConto et al., 2008; Hodell et al., 2001; Holbourn et al., 2018; Larsen et al., 1994). Interestingly, benthic foraminiferal oxygen isotopes ($\delta^{18}O$) show little long-term change during the late Miocene indicating minor ice-sheet variability, while a global decrease in benthic $\delta^{13}C$ was observed (Diester-Haass et al., 2006; Herbert et al., 2016; Hodell & Venz-Curtis, 2006). This late Miocene benthic $\delta^{13}C$ shift has to some extent been related to the aridification of interior Asia (An et al., 2001) and the expansion of C4 plants in the western Himalayan foreland basin (Galy et al., 2010; Huang et al., 2007; Quade et al., 1989; Singh et al., 2011; Vögeli et al., 2017), although the timing of the terrestrial $\delta^{13}C$ change was not synchronous across the globe or even the subcontinent (Tauxe & Feakins, 2020). There is new evidence for a decline in atmospheric CO_2 accompanying the late Miocene cooling (Tanner et al., 2020), which would favor C4 plants and in east Asia increased aridity likely resulted from the strengthening of the dry winter monsoon season at this time (Holbourn et al., 2018).

Studies of the tectonic evolution of the Himalayas and the Tibetan plateau in the late Miocene are contradictory. While several publications inferred a pulse of the Tibetan plateau uplift around 8 Ma (An et al., 2001; Li et al., 2014; Miao et al., 2012; Molnar, 2005), more recent studies suggest that the Tibetan plateau, and perhaps more importantly for the South Asian Monsoon, the Himalayan orographic barrier has been near to present elevations for at least the past 15 Myr (e.g., Clift & Webb, 2019; Ding et al., 2017) or since the mid Miocene (Gébelin et al., 2013). Sediment accumulation rates on the distal Bengal Fan, as recorded in ODP Sites 717 and 718, were high from 17 to 7 Ma, but decreased from 7 to 1 Ma (Derry & France-Lanord, 1996). Moreover, the clay mineral assemblages and elemental composition of these distal fan sediments indicated intensified chemical weathering and reduced physical erosion in the Ganges-Brahmaputra basin after 7 Ma (Clift et al., 2008; Derry & France-Lanord, 1996). Another argument against a major enhancement of tectonic uplift in the late Miocene is the relatively constant provenance of the eroded sediments supplied to the Bengal Fan over the last >17 Ma (Derry & France-Lanord, 1996; Galy et al., 2010) and to the Ninetyeast Ridge over the last 27 Ma (Ali et al., 2021).

The South Asian summer monsoon (SAM) precipitation controls the weathering regime of South Asia. For many years, it was considered that the SAM strengthened considerably at ~8–7 Ma as suggested by enhanced oceanic upwelling recorded in the Arabian Sea reflecting the strengthening of summer monsoon winds (Gupta et al., 2015; Kroon et al., 1991). However, studies investigating late Miocene monsoon intensity using various proxies in different regions rather indicated a weakening of summer monsoon rainfall intensity, as inferred for example from clay mineral compositions (Lee et al., 2019), K/Al ratios (Clift et al., 2008), seawater $\delta^{18}O$ (Steinke et al., 2010), or leaf wax δD (Huang et al., 2007). At the same time, the dry winter monsoon intensity is thought to have strengthened (Holbourn et al., 2018; Huang et al., 2007; Lee et al., 2019). The discrepancy between these interpretations may be partly caused by regional differences, for example leaf wax δD from the Indus and peninsular India exhibited little change coincident with C4 plant expansion (Feakins et al., 2020), or results from the decoupling between monsoon wind-related records and monsoon rain-related runoff, erosion, and weathering records on long timescales.

To date, all studies investigating the relationship between variations of the SAM and the erosional and weathering regime during the Miocene period have been carried out at a relatively low temporal resolution (e.g., France-Lanord et al., 1993: Myr timescale). To help improve our current understanding, we present a higher resolution record from a continuous sediment sequence with a well-constrained chronology that was recovered at IODP Site U1443 on the Ninetyeast Ridge in the southern Bay of Bengal. Age control from 9 to 5 Ma is established by tuning a low-resolution benthic stable carbon isotope record from Site U1443 (Data Set S2) to the reference section of ODP Site 1146 (Holbourn et al., 2018, 2021) and is consistent with magneto-bio-stratigraphy (Clemens et al., 2016; Figure S1). This provides a stratigraphic framework with which to compare the evolution of SAM silicate weathering inferred from changes in the clay radiogenic isotopes of Sr, Nd, and Pb with global carbon cycle and climate changes during the late Miocene.

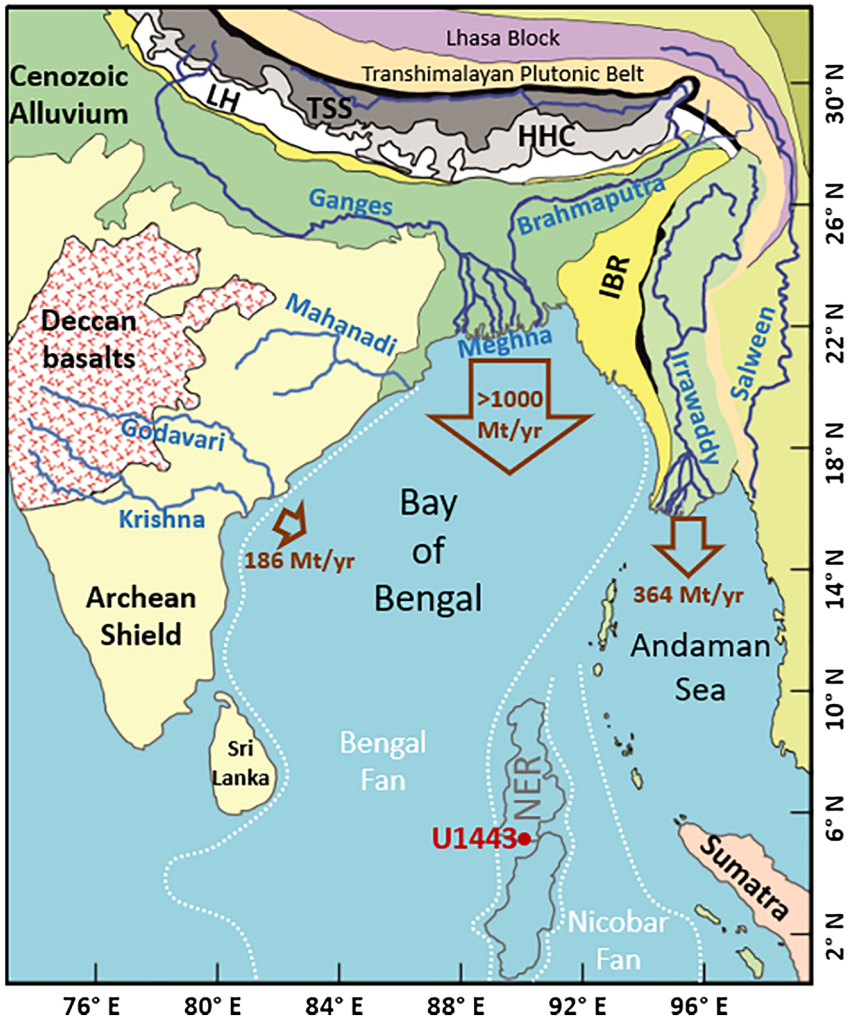

Figure 1. Map of the major geological units surrounding the Bay of Bengal taken from Bretschneider et al. (2021) after Ali et al. (2021). IODP Site U1443 is located on the Ninetyeast Ridge (NER) with the Bengal and Nicobar fans on either side. Major rivers are labeled in blue while modern sediment fluxes are given in brown (Milliman & Syvitski, 1992; Robinson et al., 2007). Lithologies: LH = Lesser Himalayas, TSS = Tethyan Sedimentary Series, HHC = High Himalayan Crystalline, and IBR = Indo Burman Ranges. Rocks of the Transhimalayan plutonic belt (TPB) are found along the Indus-Yarlung Suture marked by the thick black line.

The freshwater and sediment fluxes to the Bay of Bengal from the rivers draining the Himalayas (Ganges-Brahmaputra), the Indo-Burman Ranges (IBR) (Irrawaddy & Arakan coastal rivers), and peninsular India (Mahanadi, Godavari & Krishna) (Figure 1) are some of the largest globally (Milliman & Syvitski, 1992). The sediments produced by the erosion of the Himalayan orogeny has filled in whole basins now in Bangladesh and formed the IBR (Najman et al., 2008, 2020) and constructed the largest submarine fan system on Earth; the Bengal and Nicobar Fans (Curray et al., 2003). Deposition on the Bengal Fan has occurred since at least early Miocene times (Derry & France-Lanord, 1996; France-Lanord et al., 1993), while the Nicobar Fan to the east of the Ninetyeast Ridge did not begin to build quickly until the end of the middle Miocene (McNeill et al., 2017; Pickering et al., 2020). Under modern day conditions, the majority of sediments are delivered to the Bay of Bengal during the SAM months of June–September (Singh et al., 2007) suggesting the variability of weathering and erosion in the past was most likely related to changes in SAM precipitation. Silicate weathering amplified by the erosion of the Himalayas was potentially a fundamental driver of global climate change either directly by consuming atmospheric CO_2 during weathering reactions or indirectly by producing clays, which enhanced the sequestration of CO_2 through organic carbon burial in the deep

sea fan (France-Lanord & Derry, 1997; Galy et al., 2007, 2010; Raymo, 1994; Raymo & Ruddiman, 1992; Yang et al., 2020). A decrease in the flux and extent of weathering of terrigenous material supplied by the Indus, Mekong, and Pearl rivers since the mid Miocene indicates a decreasing or stable removal of CO_2 by Himalayan-induced silicate weathering, suggesting this was not the mechanism responsible for global Neogene cooling (Clift & Jonell, 2021). However, the enhanced silicate weathering in the mid Miocene is consistent with the timing of mid Miocene global cooling and there is evidence for an increase in the supply of clays produced by silicate weathering from the rivers draining into the Bay of Bengal over the Neogene (Ali et al., 2021).

The radiogenic isotope compositions of Sr, Nd, and Pb in rocks are a function of the rock type being crustal or mantle derived and the age (e.g., Frank, 2002). Therefore, the different lithologies surrounding the Bay of Bengal (Figure 1) have distinctive isotopic signatures, which can be used to determine the provenance of detrital material delivered to the southern Bay of Bengal (Ahmad et al., 2005; Colin et al., 1999). The IBR, being derived from Himalayan erosion and the Myanmar arc, have a Sr and Nd isotopic signature almost identical to that of the Transhimalayan plutonic belt (TPB) (Awasthi et al., 2014; Singh & France-Lanord, 2002) and have formed the western boundary of the Irrawaddy catchment since the earliest Miocene (Najman et al., 2020). Our previous work has shown that clays with an Sr, Nd, and Pb isotopic composition like those from the Irrawaddy, Brahmaputra, and Ganges rivers can explain the mixture deposited in the southern Bay of Bengal during the middle Miocene (Bretschneider et al., 2021). Here, we expand on that work to reconstruct weathering and erosion surrounding the Bay of Bengal at ~100 kyr resolution through the late Miocene from 9 to 5 Ma. We focus on the detrital clay size-fraction to minimize the effects of mineral sorting during transport, which is especially important for Sr and Pb isotopic ratios, as they vary systematically with grain size (Douglas et al., 1995; Eisenhauer et al., 1999; Garçon et al., 2014; Tütken et al., 2002). Even though Nd isotope signatures generally do not vary strongly with grain size (e.g., Tütken et al., 2002), exceptions exist, in particular in sediments from larger rivers (Bayon et al., 2015), including the Indus (Jonell et al., 2018), the Ganges (Garçon et al., 2014), and the Brahmaputra (Singh & France-Lanord, 2002). If the provenance of the detrital clay size-fraction can be constrained with Nd isotopes, Sr and Pb isotope compositions offer additional information on incongruent weathering because of large variations in the Sr and Pb isotopic composition of different mineral phases, which weather differentially (Ali et al., 2015; Blum et al., 1993; Tütken et al., 2002). As the clays are the product of silicate weathering, together these isotopic signals constrain the provenance or location of silicate weathering while providing insights into past weathering regimes and therefore climate.

2. Methods

Our study is based on sediments from IODP Site U1443 (Latitude 5°23'N, Longitude 90°21'E, and water depth ~2,930 mbsl) using nearly identical techniques to those detailed in Bretschneider et al. (2021), so only a brief description of the methods is given here. The upper Miocene sediments of U1443 are nannofossil oozes with variable amounts of foraminifers, detrital clay, biosilica, and volcanic ash (Clemens et al., 2016), and span a composite core depth from 70 to 123 m below seafloor. The age model used in this study is based on the tuning of $\delta^{13}C$ measurements of monospecific epifaunal benthic foraminifers (*Cibicidoides wuellerstorfi*) to the reference section of ODP Site 1146 (e.g., Holbourn et al., 2018, 2021) and is consistent with Site U1443 calcareous nannofossil biostratigraphy and magnetostratigraphy (Clemens et al., 2016; see Supporting Information S1 for details). Between 6 and 8 well-preserved *Cibicidoides wuellerstorfi* were picked from the >212 μm fraction and cleaned in ethanol in an ultrasonic bath after being broken into fragments. Followed by drying in an oven at 40°C, stable carbon and oxygen isotopes were measured using a Carbo-Kiel IV device coupled with a Finnigan-MAT 253 dual-inlet isotope ratio mass spectrometer (DI-IRMS) at the Leibniz Laboratory, University of Kiel. Long-term precision is better than ±0.05‰ for $\delta^{13}C$ based on an analysis of international and in-house carbonate standards and results calibrated using the National Institute of Standard and Technology (NIST) carbonate isotope standard and NBS (National Bureau of Standard) 19, and are reported on the Vienna PeeDee Belemnite (VPDB) scale. The full resolution benthic stable isotope record for the late Miocene is presented in Bolton et al. (2021).

The sedimentation rate during the late Miocene varied between 0.54 and 1.97 cm/kyr and was on average 1.36 cm/kyr. Sediment samples were washed at CEREGE over a 63 μm sieve and the fine fraction collected.

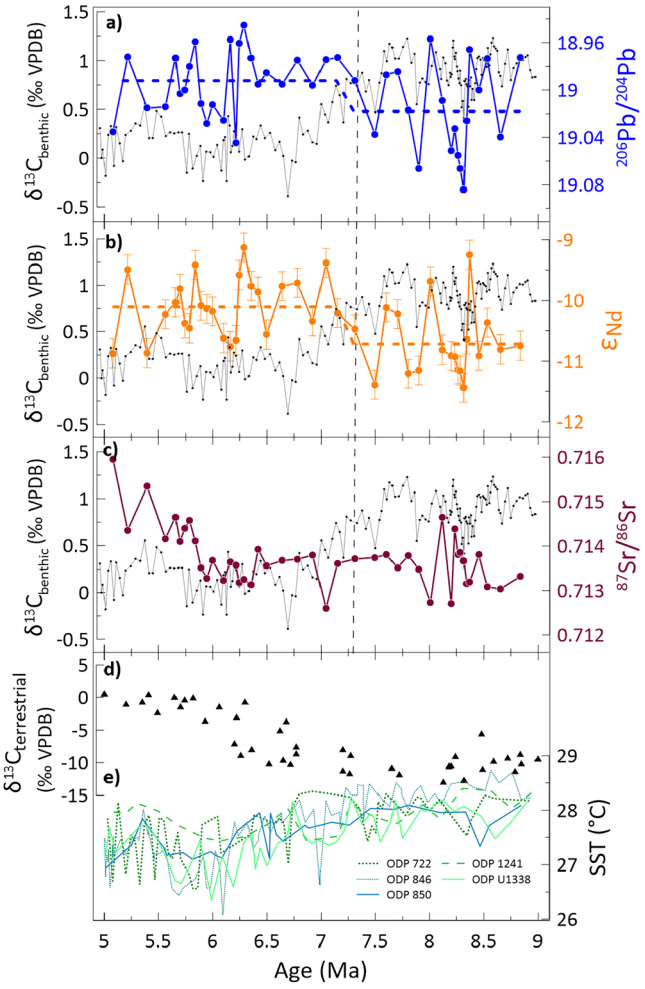

Figure 2. Radiogenic (a) Pb (blue, inverted scale), (b) Nd (orange), and (c) Sr (red) isotope compositions of U1443 clays compared to the benthic $\delta^{13}C$ signal for the interval from 9 to 5 Ma. The black dots and line show the benthic $\delta^{13}C$ measurements of this study and Lübbers et al. (2019). Nd isotopes are plotted as ε-notation; the relative deviation of the sample $^{143}Nd/^{144}Nd$ from that of the CHondritic Uniform Reservoir (CHUR, $^{143}Nd/^{144}Nd = 0.512638$). No attempt was made to correct CHUR values for decay of 147Sm since the late Miocene. The error bars represent the 2 s.d. of the repeated processing and measurement of BHVO-2 and are smaller than symbol size for Sr and Pb isotopes. The horizontal dashed lines represent the average Pb and Nd isotope compositions before and after 7.3 Ma (vertical dashed line) representing the shift to more Irrawaddy-like dominated contributions. A t-test using the software Past (Hammer et al., 2001) verified that the average values in ε_{Nd} and $^{206}Pb/^{204}Pb$ signatures before and after 7.3 Ma differed significantly from one another (p-values$_{\text{same mean}} < 0.05$); (d) shows the $\delta^{13}C$ evolution of palaeosol carbonate nodules from the Siwalik Sequence in northern Pakistan, representing the C4 plant expansion (Quade et al., 1989), and (e) represents alkenone sea surface temperature (SST) records generated for the tropics (Herbert et al., 2016; and references within).

While the coarse fraction was dried and used for micropaleontological work, the fine fraction was centrifuged, oven dried at 50°C, and sent to GEOMAR where it was processed to isolate clays by removing carbonates and authigenic Fe-Mn oxyhydroxides following a procedure modified from Gutjahr et al. (2007). Further details of the sample treatment, element purification, and isotope measurements are provided in the Supporting Information S1 and Bretschneider et al. (2021).

3. Results and Discussion

The $^{87}Sr/^{86}Sr$, ε_{Nd}, and Pb isotope compositions ($^{206}Pb/^{204}Pb$, $^{207}Pb/^{204}Pb$, $^{208}Pb/^{204}Pb$, $^{207}Pb/^{206}Pb$, and $^{208}Pb/^{206}Pb$) of the clay-sized silicate fraction are shown in Figure 2. The $^{87}Sr/^{86}Sr$ compositions vary between 0.71261 and 0.71595 over the entire time interval from 9 to 5 Ma. Between 9 and 6 Ma, the $^{87}Sr/^{86}Sr$ values exhibit little variability between 0.71261 and 0.71465 but then increase to a maximum value of 0.71595 between 6 and 5 Ma. The ε_{Nd} values range from −11.4 to −9.1, with a small step change in the average ε_{Nd} value from ∼−10.7 between 9 and 7.3 Ma to a more radiogenic average ε_{Nd} value of ∼−10.1 between 7.3 and 5 Ma. $^{206}Pb/^{204}Pb$ values vary between 18.945 and 19.084 and, similar to the ε_{Nd} values, exhibit a step change in average values at ∼7.3 Ma: The average $^{206}Pb/^{204}Pb$ signature between 9 and 7.3 Ma of ∼19.02 decreased to ∼18.99 between 7.3 and 5 Ma.

3.1. Provenance of Clays

The clays from IODP Site U1443 represent a mixture dominated by sediments from the IBR, High Himalayan Crystalline (HHC), and Tethyan Sedimentary Series (TSS) sources. Figure 3 shows the Sr and Nd isotope composition of the late Miocene U1443 clays in comparison with literature data of possible source areas and the isotopic compositions of sediments of the major rivers. The Transhimalayan Plutonic Belt (TPB including the Gangdese Batholith) is not separately defined here as an independent source area because it overlaps with the Brahmaputra sediment signatures. The TPB and TSS rocks are widely exposed in the drainage basin of the Yarlung-Tsangpo River, which flows into the Brahmaputra providing sediments with more radiogenic Nd isotope signatures. In addition to the sediments supplied by the great rivers to the Ninetyeast Ridge, fine-grained mineral dust, most likely from the deserts to the west bordering the Arabian Sea, may have contributed to the U1443 clay fraction. Although the modern dust flux (Srinivas & Sarin, 2013) is of a similar magnitude to sediment trap-derived lithogenic fluxes near the Ninetyeast Ridge (Unger et al., 2003), recent Ninetyeast Ridge sediments are clearly dominated by silicate material delivered by the giant rivers (e.g., Ahmad et al., 2005). Mineral and clay fluxes at Ocean Drilling Program (ODP) Site 758 redrilled by Site U1443 were highly elevated compared to more distal sites in the Indian Ocean (Ali et al., 2021; Hovan & Rea, 1992) by the late Miocene suggesting that dust was most likely not an important source and Site U1443 detrital material was primarily supplied by the great rivers. Moreover, sources from peninsular India or Sumatra are considered to be minor based on the isotope compositions as discussed in Bretschneider et al. (2021).

The binary mixing relationships of Nd-Sr (Figure 3), Pb-Pb (Figure 4), and Nd-Pb (Figure 5) isotope compositions between the most likely endmembers (Table S1) allow us to identify and estimate the different

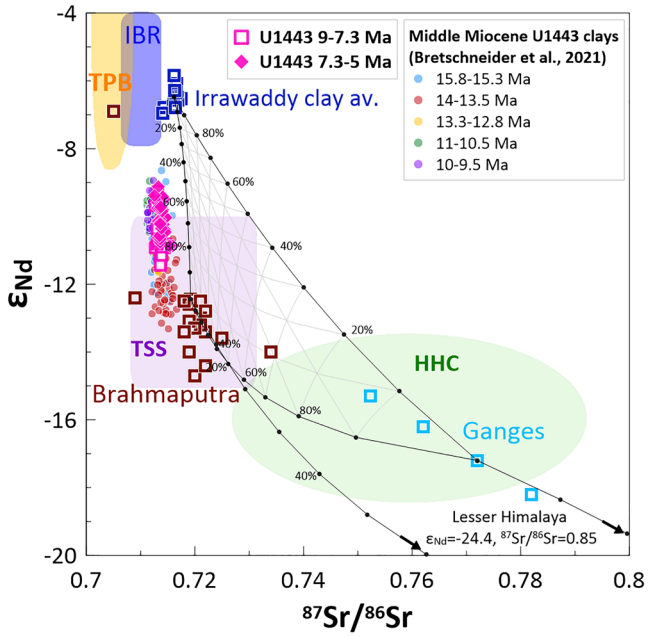

Figure 3. Strontium and neodymium isotope composition of the late Miocene clay size silicate fraction of southern Bay of Bengal sediments (Site U1443). See Figure 1 for the explanation of lithologic sources. The mixing between average Irrawaddy, Brahmaputra, and Ganges sediments was calculated in 10% increments using the endmember values in Table S1. Middle Miocene Site U1443 clay data are from Bretschneider et al. (2021).

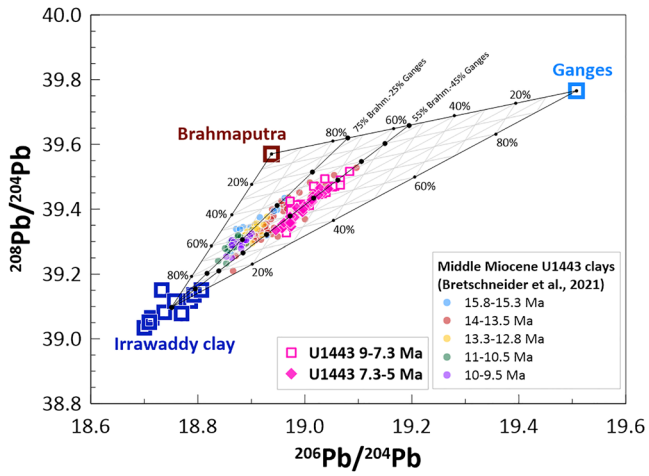

Figure 4. Lead isotope composition of the late Miocene clay size silicate fraction of southern Bay of Bengal sediments (Site U1443). The mixing between average Irrawaddy, Brahmaputra, and Ganges sediments was calculated in 10% increments using the endmember values in Table S1. The late Miocene data plot on a binary mixing line with higher Ganges contribution (45%), while most other Miocene samples plot on the binary mixing line with only 25% Ganges contribution. Middle Miocene Site U1443 clay data are from Bretschneider et al. (2021).

sediment contributions of the different major rivers to the Ninetyeast Ridge clays. To constrain and visualize mixed source contributions, ternary mixing grids were added to Figures 3–5. Data for Sr, Nd, and Pb isotope systems exist for most of the river sediments, we applied average Irrawaddy clay and average bulk Brahmaputra and Ganges sediment isotopic signatures as mixing endmembers after Bretschneider et al., (2021). In Sr-Nd isotope space, the late Miocene U1443 clays plot outside the triangle spanned by the Irrawaddy, Brahmaputra, and Ganges sediments with lower Sr isotope ratios (Figure 3). While ε_{Nd} values plot close to a mixing line between the Irrawaddy and Brahmaputra endmembers, the $^{87}Sr/^{86}Sr$ ratios are less radiogenic. A similar offset has already been discussed by Bretschneider et al. (2021) for the period between 15.8 and 9.5 Ma and has been attributed to a shift in the average source endmember signature of the clays toward less radiogenic $^{87}Sr/^{86}Sr$ ratios in the Miocene compared to the modern. We note that the large spread in $^{87}Sr/^{86}Sr$ ratios measured for Brahmaputra river sediments and the limited available data (especially for clay size fractions) may simply miss the least radiogenic part. Therefore, the mixing relationship defined by the Pb-Pb and the Nd-Pb isotope plots is more appropriate to distinguish changes in the source provenance of the clays. The plots (Figures 4 and 5) clearly demonstrate that all three endmembers contributed to the late Miocene U1443 clay Pb and Nd compositions.

The late Miocene samples define a clear linear trend on the Pb-Pb isotope plot (Figure 4) on the mixing line between Irrawaddy clay and a mixture of ~45% Ganges and ~55% Brahmaputra sources. The Irrawaddy contribution ranges from ~25% to 60%, while the mixed Himalayan contribution amounts to 40%–75%. On the Nd-Pb isotope plot (Figure 5), the binary trend is not as obvious. The Irrawaddy contribution ranges from ~20% to 55%, very close to what has been inferred from the Pb-Pb mixing plot. If a binary mixing line is drawn through the samples and the Irrawaddy endmember, the Ganges–Brahmaputra endmember mixture would again be very similar to the Pb-Pb plot reaching ~40% Ganges and ~60% Brahmaputra contributions.

Overall, the sources contributing material to the U1443 clays remained relatively stable throughout the late Miocene, which is in agreement with the relatively stable provenance of sediments supplied to the Bengal Fan since the Miocene (Blum et al., 2018; Galy et al., 2010) and of the clays delivered to the Ninetyeast Ridge over the last 27 Ma (Ali et al., 2021). Two changes of sediment sources can, however, be observed in the detrital clay radiogenic isotope record. First, late Miocene samples are systematically offset to the earlier Miocene intervals in Nd-Pb isotope space (Figure 5), and second, a step change in both average ε_{Nd} and $^{206}Pb/^{204}Pb$ values occurred at ~7.3 Ma (Figure 2).

3.2. Offset Between Middle and Late Miocene Samples—Exhumation of Lesser Himalayan Units

The late Miocene samples are offset from the middle Miocene U1443 clays (Figure 5; Bretschneider et al., 2021). This offset may be related to a shift to a higher Ganges fraction in the Ganges-Brahmaputra endmember. A 20% elevated fraction of Ganges material in the Ganges-Brahmaputra mixture in the late Miocene compared to the middle Miocene intervals (15.8–9.5 Ma) can explain this shift and may have been driven by more

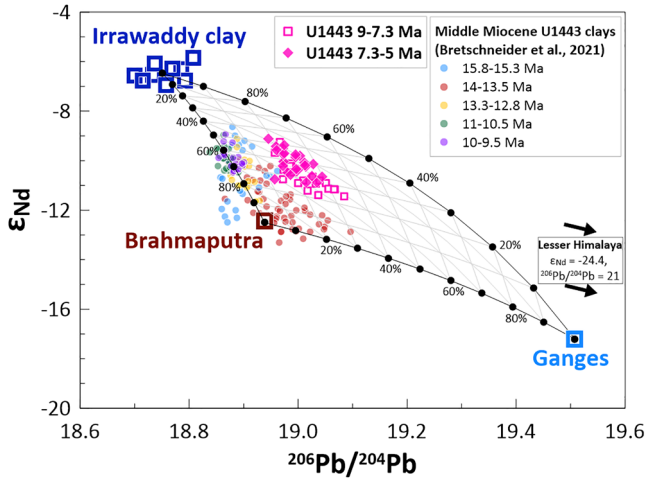

Figure 5. Neodymium and Pb isotopic compositions of the late Miocene clay size silicate fraction of southern Bay of Bengal sediments (Site U1443). The mixing between average Irrawaddy, Brahmaputra, and Ganges sediments was calculated in 10% increments using the endmember values in Table S1. The late Miocene data of this study are clearly offset from the middle Miocene samples from this site (Bretschneider et al., 2021) indicating a higher Ganges contribution for the younger interval (50%–60%) in the Ganges-Brahmaputra mixed endmember. Lesser Himalayan sediments plot far outside these bounds (as indicated by the black arrows) but contribute to the Ganges signal.

intense erosion of HHC rocks. Another possibility for the offset could be minor Lesser Himalayan (LH) contributions. If we substitute the Ganges for LH material, a contribution of 3%–10% LH material could account for the shift in the late Miocene sample composition. Since this is unrealistic and given that there must have been a Ganges contribution, it is likely that much smaller percentages of the LH component shifted the Ganges endmember toward more radiogenic Pb and Sr and less radiogenic Nd isotope compositions. The exhumation of Lesser Himalayan rocks (LH: $\varepsilon_{Nd} \sim -24.4$, $^{87}Sr/^{86}Sr \sim 0.85$, and $^{206}Pb/^{204}Pb > 19.5$; Clift et al., 2002; Singh & France-Lanord, 2002) was suggested to have started in the middle Miocene at ~16 Ma (Colleps et al., 2018). Surprisingly, in the middle Miocene U1443 record, LH signatures were virtually absent. This has been attributed to the negligible exposure of LH units in the eastern part of the Himalayas, which acts as the major watershed of the Brahmaputra. The Brahmaputra in turn dominates over the Ganges contributions in the Himalayan component in the Ninetyeast Ridge clays. However, other studies suggest that between 12 and 9 Ma LH rocks were exposed and eroding (Huyghe et al., 2001), potentially shifting the Ganges-Brahmaputra mixture toward more radiogenic Pb and Sr and less radiogenic Nd isotope compositions and thus closer to a modern "Ganges-like" signature. Provenance studies from the Siwalik Group sediments employing Nd isotopes recorded the influence of less radiogenic LH units at 11 Ma (Najman et al., 2009, 2010), around 10 Ma (Huyghe et al., 2001), and by 9.8 Ma (Mandal et al., 2019) consistent in timing with our observed shift in isotope compositions. These records indicate an increasingly less radiogenic LH fraction toward the present (Huyghe et al., 2001) with an increase around 6 Ma at some sections (Mandal et al., 2019; Najman et al., 2009). Nevertheless, the LH contribution to the clays reaching the Ninetyeast Ridge remained modest throughout the late Miocene, similar to the small contribution recorded in the NW Indian Siwaliks (Mandal et al., 2019). Thus, it was not necessarily a higher Ganges contribution but a change in the Ganges composition that may have resulted in the shift of the clay isotope composition between 9.5 and 9 Ma.

3.3. Step Change in Nd and Pb Isotope Compositions at ~7.3 Ma

The late Miocene time series of Figure 2 shows a step change in both average ε_{Nd} and $^{206}Pb/^{204}Pb$ values at ~7.3 Ma. The Nd isotope composition becomes more radiogenic, while the average Pb isotope composition decreases, both indicating an increase in Irrawaddy-like sediment contributions of about ~10% on average. These Irrawaddy-like sediments may well have been delivered from the IBR by the Arakan coast rivers known to influence the composition of surface sediments in the Bay of Bengal (Colin et al., 1999) or possibly increasing TPB contributions through the Brahmaputra, which may have taken a different course than today (paleo Brahmaputra e.g., Pickering et al., 2020). Although the change in the average value is small (but statistically significant), more radiogenic ε_{Nd} and lower $^{206}Pb/^{204}Pb$ values occurred much more frequently after 7.3 Ma and the peak unradiogenic ε_{Nd} and highest $^{206}Pb/^{204}Pb$ values were less extreme than those encountered prior to 7.3 Ma. This may hint at a reduction of the least radiogenic ε_{Nd} component, most likely the HHC or a small LH fraction, or that the Irrawaddy-like material was more continuously supplied compared to before 7.3 Ma.

This shift in clay Nd and Pb isotope compositions occurs during the global $\delta^{13}C$ decline recorded in benthic foraminifera (Figure 2). Interestingly, Galy et al. (2010) observed a trend opposite to our record in their Nd isotope compositions of the last 12 Ma on the Bengal Fan (Figure 6) although their low sampling resolution may have resulted in aliasing (only three samples younger than 7 Ma). The ε_{Nd} signatures, which are much more Himalayan dominated likely due to different source areas for the coarse material supplied to the Bengal Fan compared to the Ninetyeast Ridge clays, became less radiogenic after 7.4 Ma, attributed to an increase in HHC rock contributions (Galy et al., 2010). Galy et al. (2010) suggested that a reduction in precipitation may have led to a concentration of erosion at higher elevations of the Himalayas and consequently

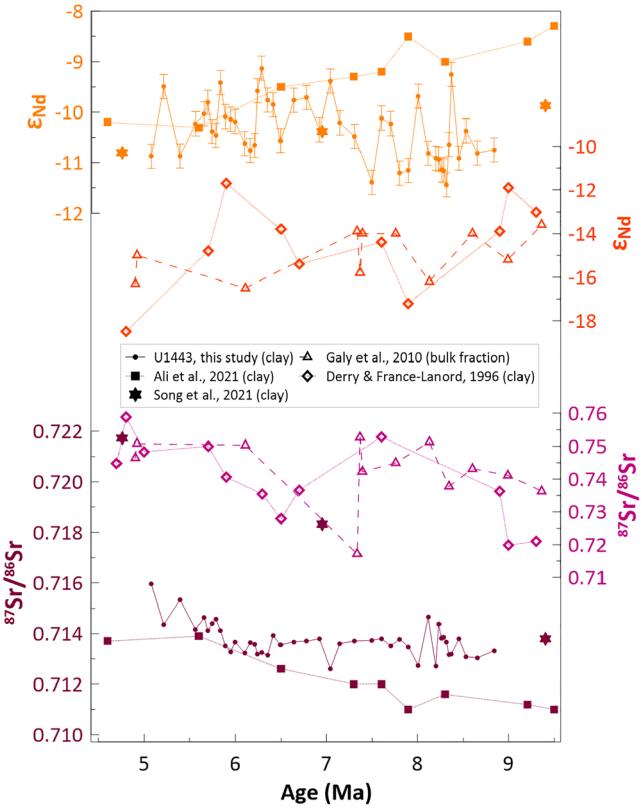

Figure 6. Evolution of U1443 clay radiogenic Sr and Nd isotope compositions compared to other studies from nearby in the Bay of Bengal. The records of Ali et al. (2021) and Song et al. (2021) are on the same scale as the U1443 data, while the records of Galy et al. (2010) and Derry and France-Lanord (1996) are displayed on a larger scale. The large differences in values are a result of the different sample locations and sediment contributions to the Bengal Fan and the Ninetyeast Ridge. Also, note that Song et al. (2021) did not treat samples specifically to remove authigenic oxides, possibly explaining the difference in Sr isotopes between studies while the Nd isotopes are similar. The error bars represent the 2 s.d. of the repeated processing and measurement of BHVO-2 and are smaller than the symbols for Sr isotopes.

enhanced the erosion of the HHC. However, the colder climate would also have resulted in less moisture in the atmosphere, hampering rainfall from reaching high elevations and promoting the observed C4 plant expansion (e.g., Quade et al., 1989; Tauxe & Feakins, 2020) as a result of increased aridity. Moreover, modern-day orographic rainfall patterns are centered above the IBR and the LH and not above the HHC (e.g., Ali et al., 2021). Instead of a higher erosion intensity of the HHC, the subtle change observed by Galy et al. (2010) could also be attributed to the onset of the erosion of LH units and a modest LH contribution resulting in a decrease of the ε_{Nd} of the mixture. These authors found this unlikely based on the lack of change in Os isotope data from the Bengal Fan, because increased LH contributions should have resulted in an increase in the $^{187}Os/^{188}Os$ signature (Galy et al., 2010). However, Os is highly concentrated in organic-rich sedimentary rocks (Colleps et al., 2018) and therefore, could be decoupled from changes in Sr and Nd provenance, in particular when the required LH contribution is small. This possibility is supported by the finding that some of the altered carbonates of the LH do not have high Os concentrations or $^{187}Os/^{188}Os$ (Colleps et al., 2018).

The coincidence of increasing Irrawaddy-like sediment contributions at ~7.3 Ma with the cooling of the global climate (Figure 2e) and the increasing aridity in the Asian interior suggests that it is reasonable to assume a climatic control on this change in sediment source. The decrease in marine $\delta^{13}C$ between ~8 and 6.5 Ma (Diester-Haass et al., 2006; Holbourn et al., 2018) accompanied the $\delta^{13}C$ increase of terrestrial records (Figure 2d), such as fossil tooth enamel, soil carbonate, or organic matter, which has been related to C4 plant expansion (Behrensmeyer et al., 2007; Cerling et al., 1997; Herbert et al., 2016; Huang et al., 2007; Quade et al., 1989). C4 plants are enriched in ^{13}C compared to C3 plants and their expansion is thus thought to have transferred significant amounts of material enriched in ^{13}C from the marine to the terrestrial carbon reservoir (Diester-Haass et al., 2006; Holbourn et al., 2018). The emerging grasslands themselves, while possibly promoted by declining levels of atmospheric CO_2 (Tanner et al., 2020), may also have favored regional aridification as a consequence of the higher albedo and lower transpiration compared to woodlands (Retallack, 2001). Moreover, grasslands and their soils serve as an important carbon and water vapor sink and therefore their expansion likely contributed to the long-term global climatic cooling (Retallack, 2001). Our records suggest that increased amounts of IBR material were weathered and eroded, implying a shift in the locus of monsoon precipitation. The locus of monsoon rains likely shifted eastward to the IBR, a region that also receives the most intense monsoon rainfall today (Damodararao et al., 2016). This is also in agreement with authigenic Nd isotope compositions on glacial-interglacial timescales investigated by Stoll et al. (2007), who found a reduction in precipitation in the northernmost reaches of the SW monsoon and an increase in precipitation over the southern Arakan coast and southern Irrawaddy drainage basin during glacial times compared to interglacials. This was interpreted to be a response to the movement of the Inter-Tropical Convergence Zone, which was driven by Northern Hemisphere cooling (Stoll et al., 2007). The Nicobar Fan had high sediment accumulation rates starting at ~9.5 Ma and persisting until ~5 Ma, when the eastern drainage route closed (Pickering et al., 2020). This high late Miocene sediment supply was attributed to the inversion of the Shillong Plateau and the westward migration of the Indo-Burman wedge, which reduced continental accommodation space and thus diverted sediments south directly to the Nicobar fan (McNeill et al., 2017; Pickering et al., 2020). The timing of changes in Nicobar fan sediment accumulation rates does not match the timing of the step change in Nd and Pb isotope compositions toward a more dominant Irrawaddy contribution at ~7.3 Ma,

which is another indication that this change was induced by climatic factors rather than tectonic ones, which would have likely operated on longer timescales than the observed changes.

3.4. $^{87}Sr/^{86}Sr$ Ratios Trace Chemical Weathering Intensity

The Sr isotope composition of detrital sediments is influenced by grain-size sorting during transport, changes in contributions from the eroded source rocks, and chemical weathering intensity on land (Blum & Erel, 2003; Tütken et al., 2002). We focus on the clay size fraction, for which sorting differences are minimal (e.g., Carter et al., 2020), to infer changes in source contributions and climatically driven weathering regimes. During the interval from 9 to 5 Ma, Nd and Pb isotope compositions show some variability and a step change toward more IBR-dominated sources at 7.3 Ma, which is not mirrored by the Sr isotope compositions (Figure 2). The $^{87}Sr/^{86}Sr$ ratios remained markedly invariant between 9 and 6 Ma and then increased significantly (by ~0.003) from 6 to 5 Ma. This decoupling from Nd and Pb patterns indicates that late Miocene changes in the Sr isotope composition were not driven by changes in source contribution but more likely by variations in incongruent weathering and in chemical weathering intensity. The change in provenance observed for Nd and Pb isotopes was likely overprinted by the weathering effect for $^{87}Sr/^{86}Sr$. Moreover, the radiogenic Sr composition of modern Irrawaddy clays and Brahmaputra sediments is very similar, while the Miocene clays are slightly less radiogenic than these (Figure 3), highlighting that Sr isotopes are less useful to track source provenance compared to the highly particle reactive elements Nd and Pb because of the high water/rock concentration ratios and the mobility of Sr. Clays, in contrast to coarser sediments, incorporate a substantial fraction of the ions dissolved in the water present during their alteration and thus also take on the isotopic composition of dissolved elements (Bayon et al., 2016). Sr is more susceptible to such changes given that dissolved Sr concentrations in river waters are relatively high compared to those of Nd and Pb (e.g., Indus River: 300 ppb Sr vs. 3.2 ppt Nd; Goldstein & Jacobsen, 1987). During weak chemical weathering, the first mineral phase reacting with water is usually plagioclase, which releases relatively low $^{87}Sr/^{86}Sr$ signatures (Douglas et al., 1995). When chemical weathering becomes stronger, micas release Sr with high $^{87}Sr/^{86}Sr$. This would consequently shift the isotopic composition of the altered clays toward less radiogenic values during weak chemical weathering and toward more radiogenic values during stronger chemical weathering (Derry & France-Lanord, 1996). The marked increase in clay $^{87}Sr/^{86}Sr$ from 6 to 5 Ma, therefore, implies an increase in chemical weathering intensity.

Another factor possibly affecting the Sr isotope composition of the clays is variable contributions from weathering of the extremely radiogenic metamorphic rocks of the Himalayas, which can be found in both the High Himalayan Crystalline Series and the Lesser Himalayan Crystalline Series lithologies (Vannay et al., 2004). During the collision of India with Asia, high-grade metamorphism and partial melting of the rocks mobilized radiogenic Sr of K-rich minerals into Na- and Ca-rich minerals that weather much more easily (Edmond, 1992). The erosion of rocks containing these highly radiogenic minerals ($^{87}Sr/^{86}Sr > 0.720$) has been suggested to be responsible for the significant increase in $^{87}Sr/^{86}Sr$ values of the global ocean since 40 Ma (Oliver et al., 2003; Raymo & Ruddiman, 1992; Richter et al., 1992). Even though the weathering of the radiogenic metamorphic rocks represents a possible influence on the Sr isotope composition of our U1443 clays, none of the records point to a particular event responsible for intensified HHC or LH erosion at 6 Ma. As potential indicators, we would have expected shifts of the other isotope systems toward more HHC or LH signatures. Since this was not the case, it is most likely that an increased chemical weathering intensity was the major factor responsible for the increased Sr isotope signature of clays transported to Site U1443.

The observed shift in $^{87}Sr/^{86}Sr$ of ~0.003 between 6 and 5 Ma is somewhat smaller than the variability in earlier Miocene intervals recorded by Bretschneider et al. (2021), who found variations of up to ~0.005 in $^{87}Sr/^{86}Sr$ within only 500 kyr in the middle Miocene. These were interpreted to reflect changes in the balance of source contributions due to shifts of weathering regimes on land. However, the increase in the late Miocene is very prominent, given the consistency of the isotope compositions during the 4 million years prior to the change. A similar increase in $^{87}Sr/^{86}Sr$ during this period was hinted at in the low resolution data from ODP Site 758 that was redrilled by U1443 (Figure 6; Ali et al., 2021). Similar amplitude radiogenic spikes of +0.003 in the global average riverine sediment $^{87}Sr/^{86}Sr$ of the last 250 kyr have also been attributed to changes in weathering regime caused by accelerated weathering of biotite following deglaciations (Blum &

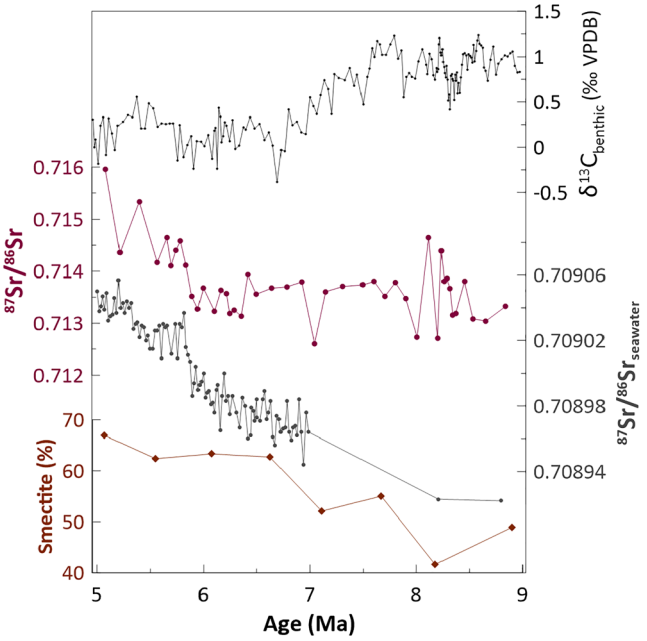

Figure 7. Comparison of the benthic $\delta^{13}C$ record (this study and Lübbers et al., 2019), detrital clay Sr isotope composition, seawater Sr isotope evolution from 9 to 5 Ma (Farrell et al., 1995; Hodell et al., 1989), and smectite abundance at ODP Site 758 (Ali et al., 2021). Note the different amplitudes of seawater and clay Sr isotope increases.

Erel, 1995). We consequently attribute the observed shift from 6 to 5 Ma to an enhancement in chemical weathering intensity.

3.5. Weathering Regimes and SAM Intensity

The increase in $^{87}Sr/^{86}Sr$ ratios of Ninetyeast Ridge clays from 6 to 5 Ma most likely resulted from an intensification of chemical weathering. An increase in the abundance of the secondary clay mineral smectite at this location in the late Miocene (Ali et al., 2021) supports this hypothesis (Figure 7). However, the increase in smectite abundance was strongest between ~8 and 6.5 Ma and remained at a high level until 5 Ma. Derry and France-Lanord (1996) also observed an increase in smectite abundance compared to primary clay minerals after 7 Ma on the distal Bengal Fan. They interpreted the high Sr isotope values ($^{87}Sr/^{86}Sr$ increase of ~0.02) to result from intensified chemical weathering of radiogenic silicates. Floodplain weathering, especially of micas containing highly radiogenic Sr, would have produced smectite, and thus may have resulted in more radiogenic Sr isotope signatures of the clays (Derry & France-Lanord, 1996). This is also the most likely explanation for the clear increase in $^{87}Sr/^{86}Sr$ ratios of the U1443 clays after 6 Ma given that these clays are dominated (>60%) by smectite.

Although the global cooling of the late Miocene resulted in ephemeral glaciations (Holbourn et al., 2018), no significant drop in sea level occurred to cause increased floodplain area and enhance chemical weathering. Instead the interplay between high sediment supply, as recorded by the Bengal and Nicobar Fans (Pickering et al., 2020), and grasslands increasing soil thickness may have provided the extra reaction space. Grassland soils also accommodate much higher internal mineral surface areas prone to weathering compared to woodland or desert soils (Retallack, 2001). Thus, the formation of thick horizons of soils with crumb peds due to the appearance of tall sod grasslands at 7–6 Ma (Figure 2d) likely accelerated chemical weathering rates (Retallack, 2001). This biological forcing may have contributed to increased chemical weathering intensities seen in the rise in Sr isotope composition and secondary clay abundance.

While global cooling was reported from 7 to 5.5 Ma (Figure 2e; Herbert et al., 2016; Holbourn et al., 2018; Jöhnck et al., 2020), oxygen isotopes and Mg/Ca measurements of mixed layer foraminifera indicated a warming from 5.5 Ma in the Andaman Sea reflecting intensified cross-equatorial transport of heat and moisture, which likely led to an increased summer monsoon precipitation during the warm stages after 5.5 Ma (Jöhnck et al., 2020). This sea surface temperature warming and increased SAM intensity after 5.5 Ma may be another important factor contributing to the increase in chemical weathering.

3.6. Implications for the Marine Sr Isotope Evolution

The rise in U1443 clay Sr isotope compositions coincided with the increase in global seawater $^{87}Sr/^{86}Sr$ between 5.5 and 4.5 Ma (Hodell et al., 1989) and between 6.1 and 4.9 Ma recorded at ODP Site 758 (Figure 7; Farrell et al., 1995). This late Miocene/early Pliocene increase in Sr isotope composition was part of the overall increase in marine $^{87}Sr/^{86}Sr$ recorded for the last 40 Myr (Richter et al., 1992). Hodell et al. (1989) related the rise in $^{87}Sr/^{86}Sr$ signature to an increase in the dissolved Sr riverine flux to the oceans and/or to an increase in the average Sr isotope composition of river water, which may have been connected to increased chemical denudation rates of the continents and shelves. Derry and France-Lanord (1996) argued for the latter scenario with their record pointing at a decrease in Sr flux and an increase in global mean $^{87}Sr/^{86}Sr$ of rivers due to high weathering intensity. The increase in detrital clay Sr isotope composition in our record as well as in others supports the argument that the change in mean $^{87}Sr/^{86}Sr$ composition of Himalayan Rivers affected the ocean's Sr isotope composition and may therefore at least partly have been responsible for the rise in seawater $^{87}Sr/^{86}Sr$ in the late Miocene/early Pliocene. Since high chemical weathering rates promote

the drawdown of CO_2, rising Sr isotope compositions suggest the cooling climate observed in the time interval between 6 and 5.5 Ma may have resulted from increased chemical weathering in the core region of SAM precipitation. In contrast, a decreasing or stable removal of CO_2 by Himalayan-induced silicate weathering is indicated by the elemental composition of material deposited by the Indus, Mekong, and Pearl rivers since the mid Miocene (Clift & Jonell, 2021). Although this suggests that enhanced silicate weathering caused by Himalayan-Tibetan erosion was not the mechanism responsible for late Miocene cooling, a complete budget of clays produced by silicate weathering is required including those produced by enhanced weathering in situ (Yang et al., 2020) and not transported and deposited by rivers.

4. Conclusions

A 100 kyr resolution record of the detrital clay radiogenic Sr, Nd, and Pb isotope composition of sediments from the southern Bay of Bengal for the late Miocene/earliest Pliocene from 9 to 5 Ma indicates an overall stable mixture of the sources of the Ninetyeast Ridge clays, which include contributions from the High Himalayan Crystalline, the Tethyan Sedimentary Series, and the Indo-Burman Ranges. The Himalayan contribution, represented by sediments delivered by the Ganges and Brahmaputra Rivers, became more Ganges-dominated than during the earlier Miocene, which likely reflects an increasing contribution from High Himalayan Crystalline or Lesser Himalayan rocks. A step change in Nd and Pb isotope compositions at ~7.3 Ma, contemporaneous with the final phase of the global marine benthic $\delta^{13}C$ decline, reflects higher Irrawaddy-like contributions connected to a climatically driven eastward shift in precipitation patterns and a more focused weathering and erosion of the Indo-Burman Ranges. The variability of Sr isotope compositions was decoupled from Nd and Pb isotope signatures and therefore indicates shifts in the weathering regime. A prominent increase in Sr isotope compositions between 6 and 5 Ma suggests increased chemical weathering intensity in the Ganges-Brahmaputra and Irrawaddy basins, which may have resulted from the expansion of C4 grasslands providing a larger mineral surface area for chemical weathering rather than an increase in South Asian summer monsoon intensity. The rise of the clay $^{87}Sr/^{86}Sr$ signature coincided with the major late Miocene/early Pliocene increase in global seawater Sr isotope composition suggesting that the change in the composition of Himalayan riverine inputs due to enhanced chemical weathering intensity may also have affected the global ocean Sr isotope signature between 6 and 5 Ma.

Data Availability Statement

The data presented in this study are included in the Supporting Information S1 and all new data are freely available on the PANGAEA data repository (https://doi.pangaea.de/10.1594/PANGAEA.932921).

Acknowledgments
This research used samples and data provided by the International Ocean Discovery Program and was funded by the German Research Foundation (DFG) (grants HA 5751/6-1 & -2). C. T. Bolton acknowledges funding from the French ANR project iMonsoon (ANR-16-CE01-0004-01) and IODP France. W. Kuhnt acknowledges funding from the DFG (grant Ku649/36-1). We especially thank Jutta Heinze for her help in the laboratory, Chris Siebert for maintaining the Nu, and Marcus Gutjahr for assistance with Pb and Nd isotope measurements on the Neptune Plus MC-ICP-MS. Neeraj Awasthi, Peter Clift, and associate editor Sarah Feakins are acknowledged for their highly constructive comments which significantly improved the manuscript.
Open access funding enabled and organized by Projekt DEAL.

References

Ahmad, S. M., Anil Babu, G., Padmakumari, V. M., Dayal, A. M., Sukhija, B. S., & Nagabhushanam, P. (2005). Sr, Nd isotopic evidence of terrigenous flux variations in the Bay of Bengal: Implications of monsoons during the last ~34,000 years. *Geophysical Research Letters*, *32*. https://doi.org/10.1029/2005gl024519

Ali, S., Hathorne, E. C., & Frank, M. (2021). Persistent provenance of South Asian monsoon-induced silicate weathering over the past 27 million years. *Paleoceanography and Paleoclimatology*, *36*(3). https://doi.org/10.1029/2020PA003909

Ali, S., Hathorne, E. C., Frank, M., Gebregiorgis, D., Stattegger, K., Sumpf, R., et al. (2015). South Asian monsoon history over the past 60 kyr recorded by radiogenic isotopes and clay mineral assemblages in the Andaman Sea. *Geochemistry, Geophysics, Geosystems*, *16*, 505–521. https://doi.org/10.1002/2014gc005586

An, Z., Kutzbach, J. E., Prell, W. L., & Porter, S. C. (2001). Evolution of Asian monsoons and phased uplift of the Himalaya-Tibetan plateau since Late Miocene times. *Nature*, *411*, 62–66.

Awasthi, N., Ray, J. S., Singh, A. K., Band, S. T., & Rai, V. K. (2014). Provenance of the Late Quaternary sediments in the Andaman Sea: Implications for monsoon variability and ocean circulation. *Geochemistry, Geophysics, Geosystems*, *15*, 3890–3906. https://doi.org/10.1002/2014gc005462

Bayon, G., Skonieczny, C., Delvigne, C., Toucanne, S., Bermell, S., Ponzevera, E., & André, L. (2016). Environmental Hf–Nd isotopic decoupling in World river clays. *Earth and Planetary Science Letters*, *438*, 25–36. https://doi.org/10.1016/j.epsl.2016.01.010

Bayon, G., Toucanne, S., Skonieczny, C., André, L., Bermell, S., Cheron, S., et al. (2015). Rare earth elements and neodymium isotopes in world river sediments revisited. *Geochimica et Cosmochimica Acta*, *170*, 17–38. https://doi.org/10.1016/j.gca.2015.08.001

Behrensmeyer, A. K., Quade, J., Cerling, T. E., Kappelman, J., Khan, I. A., Copeland, P., et al. (2007). The structure and rate of late Miocene expansion of C4 plants: Evidence from lateral variation in stable isotopes in paleosols of the Siwalik Group, northern Pakistan. *The Geological Society of America Bulletin*, *119*, 1486–1505. https://doi.org/10.1130/b26064.1

Blum, J. D., & Erel, Y. (1995). A silicate weathering mechanism linking increases in marine 87Sr/86Sr with global glaciation. *Nature*, *373*, 415–418. https://doi.org/10.1038/373415a0

Blum, J. D., & Erel, Y. (2003). Radiogenic Isotopes in Weathering and Hydrology. *Treatise on Geochemistry*, *5*, 365–392. https://doi.org/10.1016/b0-08-043751-6/05082-9

Blum, J. D., Erel, Y., & Brown, K. (1993). 87Sr/86Sr ratios of Sierra Nevada stream waters: Implications for relative mineral weathering rates. *Geochimica et Cosmochimica Acta*, *57*, 5019–5025. https://doi.org/10.1016/s0016-7037(05)80014-6

Blum, M., Rogers, K., Gleason, J., Najman, Y., Cruz, J., & Fox, L. (2018). Allogenic and autogenic signals in the stratigraphic record of the deep-sea Bengal Fan. *Scientific Reports*, *8*(1), 7973. https://doi.org/10.1038/s41598-018-25819-5

Bolton, C. T., Gray, E., Kuhnt, W., Holbourn, A. E., Lübbers, J., Grant, K., et al. (2021). Secular and orbital-scale variability of equatorial Indian Ocean summer monsoon winds during the late Miocene (preprint). *Climate of the Past Discussions*. https://doi.org/10.5194/cp-2021-77

Bretschneider, L., Hathorne, E. C., Huang, H., Lübbers, J., Kochhann, K. G., Holbourn, A., et al. (2021). Provenance and weathering of clays delivered to the Bay of Bengal during the middle Miocene: Linkages to tectonics and monsoonal climate. *Paleoceanography and Paleoclimatology*, *36*, e2020PA003917. https://doi.org/10.1029/2020pa003917

Burke, K., Williams, J., Chandler, M., Haywood, A., Lunt, D., & Otto-Bliesner, B. (2018). Pliocene and Eocene provide best analogs for near-future climates. *Proceedings of the National Academy of Sciences*, *115*, 13288–13293. https://doi.org/10.1073/pnas.1809600115

Carter, S. C., Griffith, E. M., Clift, P. D., Scher, H. D., & Dellapenna, T. M. (2020). Clay-fraction strontium and neodymium isotopes in the Indus Fan: Implications for sediment transport and provenance. *Geological Magazine*, *157*, 879–894. https://doi.org/10.1017/s0016756820000394

Cerling, T. E., Harris, J. M., MacFadden, B. J., Leakey, M. G., Quade, J., Eisenmann, V., & Ehleringer, J. R. (1997). Global vegetation change through the Miocene/Pliocene boundary. *Nature*, *389*, 153–158. https://doi.org/10.1038/38229

Clemens, S., Kuhnt, W., LeVay, L., Anand, P., Ando, T., Bartol, M., et al. (2016). Site U1443. Indian Monsoon Rainfall. In *Proceedings of the international ocean discovery program* (pp. 1–41).

Clift, P. D., Hodges, K. V., Heslop, D., Hannigan, R., Van Long, H., & Calves, G. (2008). Correlation of Himalayan exhumation rates and Asian monsoon intensity. *Nature Geoscience*, *1*, 875–880. https://doi.org/10.1038/ngeo351

Clift, P. D., & Jonell, T. N. (2021). Himalayan-Tibetan erosion is not the cause of Neogene Global Cooling. *Geophysical Research Letters*, e2020GL087742. https://doi.org/10.1029/2020gl087742

Clift, P. D., Lee, J. I., Hildebrand, P., Shimizu, N., Layne, G. D., Blusztajn, J., et al. (2002). Nd and Pb isotope variability in the Indus River System: Implications for sediment provenance and crustal heterogeneity in the Western Himalaya. *Earth and Planetary Science Letters*, *200*, 91–106. https://doi.org/10.1016/s0012-821x(02)00620-9

Clift, P. D., & Webb, A. G. (2019). A history of the Asian monsoon and its interactions with solid Earth tectonics in Cenozoic South Asia. In M. P. Searle, & P. J. Treloar (Eds.), *Himalayan tectonics: A modern synthesis* (pp. 631–652). Special Publications, 483, Geological Society. https://doi.org/10.1144/SP483.1

Colin, C., Turpin, L., Bertaux, J., Desprairies, A., & Kissel, C. (1999). Erosional history of the Himalayan and Burman ranges during the last two glacial-interglacial cycles. *Earth and Planetary Science Letters*, *171*, 647–660. https://doi.org/10.1016/s0012-821x(99)00184-3

Colleps, C. L., McKenzie, N. R., Stockli, D. F., Hughes, N. C., Singh, B. P., Webb, A. A. G., et al. (2018). Zircon (U-Th)/He thermochronometric constraints on Himalayan Thrust Belt Exhumation, Bedrock Weathering, and Cenozoic Seawater Chemistry. *Geochemistry, Geophysics, Geosystems*, *19*, 257–271. https://doi.org/10.1002/2017gc007191

Curray, J. R., Emmel, F. J., & Moore, D. G. (2003). The Bengal Fan: Morphology, geometry, stratigraphy, history and processes. *Marine and Petroleum Geology*, *19*, 1191–1223.

Damodararao, K., Singh, S. K., Rai, V. K., Ramaswamy, V., & Rao, P. S. (2016). Lithology, Monsoon and Sea-Surface Current Control on Provenance, dispersal and deposition of sediments over the Andaman Continental Shelf. *Frontiers in Marine Science*, *3*, 1–15. https://doi.org/10.3389/fmars.2016.00118

DeConto, R. M., Pollard, D., Wilson, P. A., Pälike, H., Lear, C. H., & Pagani, M. (2008). Thresholds for Cenozoic bipolar glaciation. *Nature*, *455*, 652–656. https://doi.org/10.1038/nature07337

Derry, L. A., & France-Lanord, C. (1996). Neogene Himalayan weathering history and river 87Sr/86Sr: Impact on the marine Sr record. *Earth and Planetary Science Letters*, *142*, 59–74. https://doi.org/10.1016/0012-821x(96)00091-x

Diester-Haass, L., Billups, K., & Emeis, K. C. (2006). Late Miocene carbon isotope records and marine biological productivity: Was there a (dusty) link? *Paleoceanography*, *21*.

Ding, L., Spicer, R., Yang, J., Xu, Q., Cai, F., Li, S., et al. (2017). Quantifying the rise of the Himalaya orogen and implications for the South Asian monsoon. *Geology*, *45*, 215–218. https://doi.org/10.1130/g38583.1

Douglas, G. B., Gray, C. M., Hart, B. T., & Beckett, R. (1995). A strontium isotopic investigation of the origin of suspended particulate matter (SPM) in the Murray-Darling River system, Australia. *Geochimica et Cosmochimica Acta*, *59*, 3799–3815. https://doi.org/10.1016/0016-7037(95)00266-3

Dupont, L. M., Rommerskirchen, F., Mollenhauer, G., & Schefuß, E. (2013). Miocene to Pliocene changes in South African hydrology and vegetation in relation to the expansion of C4 plants. *Earth and Planetary Science Letters*, *375*, 408–417. https://doi.org/10.1016/j.epsl.2013.06.005

Edmond, J. (1992). Himalayan tectonics, weathering processes, and the strontium isotope record in marine limestones. *Science*, *258*, 1594–1597. https://doi.org/10.1126/science.258.5088.1594

Eisenhauer, A., Meyer, H., Rachold, V., Hansen, B. T., Spielhagen, R. F., Tütken, T., et al. (1999). Grain size separation and sediment mixing in Arctic Ocean sediments: Evidence from the strontium isotope systematic. *Chemical Geology*, *158*, 173–188. https://doi.org/10.1016/s0009-2541(99)00026-1

Farrell, J. W., Clemens, S. C., & Gromet, L. P. (1995). Improved chronostratigraphic reference curve of late Neogene seawater 87Sr/86Sr. *Geology*, *23*, 403–406. https://doi.org/10.1130/0091-7613(1995)023<0403:icrcol>2.3.co;2

Feakins, S. J., Liddy, H. M., Tauxe, L., Galy, V., Feng, X., Tierney, J. E., et al. (2020). Miocene C4 grassland expansion as recorded by the Indus Fan. *Paleoceanography and Paleoclimatology*, *35*(6), e2020PA003856. https://doi.org/10.1029/2020pa003856

France-Lanord, C., Derry, L., & Michard, A. (1993). Evolution of the Himalaya since Miocene time: Isotopic and sedimentological evidence from the Bengal Fan. *Geological Society, London, Special Publications*, *74*, 603–621. https://doi.org/10.1144/gsl.sp.1993.074.01.40

France-Lanord, C., & Derry, L. A. (1997). Organic carbon burial forcing of the carbon cycle from Himalayan erosion. *Nature*, *390*, 65–67. https://doi.org/10.1038/36324

Frank, M. (2002). Radiogenic isotopes: Tracers of past ocean circulation and erosional input. *Reviews of Geophysics*, *40*(1), 1–1. https://doi.org/10.1029/2000rg000094

Galy, V., France-Lanord, C., Beyssac, O., Faure, P., Kudrass, H., & Palhol, F. (2007). Efficient organic carbon burial in the Bengal fan sustained by the Himalayan erosional system. *Nature*, *450*, 407–410. https://doi.org/10.1038/nature06273

Galy, V., France-Lanord, C., Peucker-Ehrenbrink, B., & Huyghe, P. (2010). Sr–Nd–Os evidence for a stable erosion regime in the Himalaya during the past 12 Myr. *Earth and Planetary Science Letters*, *290*, 474–480. https://doi.org/10.1016/j.epsl.2010.01.004

Garçon, M., Chauvel, C., France-Lanord, C., Limonta, M., & Garzanti, E. (2014). Which minerals control the Nd–Hf–Sr–Pb isotopic compositions of river sediments? *Chemical Geology*, *364*, 42–55. https://doi.org/10.1016/j.chemgeo.2013.11.018

Gébelin, A., Mulch, A., Teyssier, C., Jessup, M. J., Law, R. D., & Brunel, M. (2013). The Miocene elevation of Mount Everest. *Geology*, *41*(7), 799–802. https://doi.org/10.1130/g34331.1

Goldstein, S. L., & Jacobsen, S. B. (1987). The Nd and Sr isotopic systematics of river-water dissolved material: Implications for the sources of Nd and Sr in seawater. *Chemical Geology*, *66*, 245–272. https://doi.org/10.1016/0168-9622(87)90045-5

Gupta, A. K., Yuvaraja, A., Prakasam, M., Clemens, S. C., & Velu, A. (2015). Evolution of the South Asian monsoon wind system since the late Middle Miocene. *Palaeogeography, Palaeoclimatology, Palaeoecology*, *438*, 160–167. https://doi.org/10.1016/j.palaeo.2015.08.006

Gutjahr, M., Frank, M., Stirling, C. H., Klemm, V., van de Flierdt, T., & Halliday, A. N. (2007). Reliable extraction of a deepwater trace metal isotope signal from Fe–Mn oxyhydroxide coatings of marine sediments. *Chemical Geology*, *242*, 351–370. https://doi.org/10.1016/j.chemgeo.2007.03.021

Hammer, Ø., Harper, D. A., & Ryan, P. D. (2001). PAST: Paleontological statistics software package for education and data analysis. *Palaeontologia Electronica*, *4*, 9.

Herbert, T. D., Lawrence, K. T., Tzanova, A., Peterson, L. C., Caballero-Gill, R., & Kelly, C. S. (2016). Late Miocene global cooling and the rise of modern ecosystems. *Nature Geoscience*, *9*, 843–847. https://doi.org/10.1038/ngeo2813

Hodell, D. A., Curtis, J. H., Sierro, F. J., & Raymo, M. E. (2001). Correlation of late Miocene to early Pliocene sequences between the Mediterranean and North Atlantic. *Paleoceanography*, *16*, 164–178. https://doi.org/10.1029/1999pa000487

Hodell, D. A., Mueller, P. A., McKenzie, J. A., & Mead, G. A. (1989). Strontium isotope stratigraphy and geochemistry of the late Neogene Ocean. *Earth and Planetary Science Letters*, *92*, 165–178. https://doi.org/10.1016/0012-821x(89)90044-7

Hodell, D. A., & Venz-Curtis, K. A. (2006). Late Neogene history of deepwater ventilation in the Southern Ocean. *Geochemistry, Geophysics, Geosystems*, *7*. https://doi.org/10.1029/2005gc001211

Holbourn, A., Kuhnt, W., Clemens, S. C., & Heslop, D. (2021). A ~12 Myr Miocene Record of East Asian Monsoon variability from the South China Sea. *Paleoceanography and Paleoclimatology*, *36*(7). https://doi.org/10.1029/2021PA004267

Holbourn, A. E., Kuhnt, W., Clemens, S. C., Kochhann, K. G. D., Johnck, J., Lubbers, J., & Andersen, N. (2018). Late Miocene climate cooling and intensification of southeast Asian winter monsoon. *Nature Communications*, *9*, 1584. https://doi.org/10.1038/s41467-018-03950-1

Hovan, S. A., & Rea, D. K. (1992). The Cenozoic record of continental mineral deposition on Broken and Ninetyeast Ridges, Indian Ocean: Southern African aridity and sediment delivery from the Himalayas. *Paleoceanography*, *7*(6), 833–860. https://doi.org/10.1029/92pa02176

Huang, Y., Clemens, S. C., Liu, W., Wang, Y., & Prell, W. L. (2007). Large-scale hydrological change drove the late Miocene C4 plant expansion in the Himalayan foreland and Arabian Peninsula. *Geology*, *35*, 531. https://doi.org/10.1130/g23666a.1

Huyghe, P., Galy, A., Mugnier, J.-L., & France-Lanord, C. (2001). Propagation of the thrust system and erosion in the Lesser Himalaya: Geochemical and sedimentological evidence. *Geology*, *29*, 1007–1010. https://doi.org/10.1130/0091-7613(2001)029<1007:pottsa>2.0.co;2

Jöhnck, J., Kuhnt, W., Holbourn, A., & Andersen, N. (2020). Variability of the Indian Monsoon in the Andaman Sea across the Miocene-Pliocene transition. *Paleoceanography and Paleoclimatology*, *35*, e2020PA003923. https://doi.org/10.1029/2020pa003923

Jonell, T. N., Li, Y., Blusztajn, J., Giosan, L., & Clift, P. D. (2018). Signal or noise? Isolating grain size effects on Nd and Sr isotope variability in Indus delta sediment provenance. *Chemical Geology*, *485*, 56–73. https://doi.org/10.1016/j.chemgeo.2018.03.036

Kroon, D., Steens, T., & Troelstra, S. R. (1991). Onset of monsoonal related upwelling in the western Arabian Sea as revealed by planktonic foraminifers. *Proceedings of the Ocean Drilling Program, Scientific Results*, *117*, 257–263. https://doi.org/10.2973/odp.proc.sr.117.126.1991

Larsen, H., Saunders, A., Clift, P., Beget, J., Wei, W., & Spezzaferri, S. (1994). Seven million years of glaciation in Greenland. *Science*, *264*, 952–955. https://doi.org/10.1126/science.264.5161.952

Lee, J., Kim, S., Lee, J. I., Cho, H. G., Phillips, S. C., & Khim, B.-K. (2019). Monsoon-influenced variation of clay mineral compositions and detrital Nd-Sr isotopes in the western Andaman Sea (IODP Site U1447) since the late Miocene. *Palaeogeography, Palaeoclimatology, Palaeoecology*, *538*, 109339.

Li, J., Fang, X., Song, C., Pan, B., Ma, Y., & Yan, M. (2014). Late Miocene–Quaternary rapid stepwise uplift of the NE Tibetan Plateau and its effects on climatic and environmental changes. *Quaternary Research*, *81*, 400–423. https://doi.org/10.1016/j.yqres.2014.01.002

Lübbers, J., Kuhnt, W., Holbourn, A. E., Bolton, C. T., Gray, E., Usui, Y., et al. (2019). The Middle to Late Miocene "Carbonate Crash" in the Equatorial Indian Ocean. *Paleoceanography and Paleoclimatology*, *34*, 813–832. https://doi.org/10.1029/2018pa003482

Mandal, S. K., Scherler, D., Romer, R. L., Burg, J., Guillong, M., & Schleicher, A. M. (2019). Multi-proxy isotopic and geochemical analysis of the Siwalik sediments in NW India: Implication for the Late Cenozoic tectonic evolution of the Himalaya. *Tectonics*, 2018TC005200. https://doi.org/10.1029/2018TC005200

McNeill, L. C., Dugan, B., Backman, J., Pickering, K. T., Pouderoux, H. F. A., Henstock, T. J., et al. (2017). Understanding Himalayan erosion and the significance of the Nicobar Fan. *Earth and Planetary Science Letters*, *475*, 134–142. https://doi.org/10.1016/j.epsl.2017.07.019

Miao, Y., Herrmann, M., Wu, F., Yan, X., & Yang, S. (2012). What controlled Mid–Late Miocene long-term aridification in Central Asia?—Global cooling or Tibetan Plateau uplift: A review. *Earth-Science Reviews*, *112*, 155–172. https://doi.org/10.1016/j.earscirev.2012.02.003

Milliman, J. D., & Syvitski, J. P. (1992). Geomorphic/tectonic control of sediment discharge to the ocean: The importance of small mountainous rivers. *The Journal of Geology*, *100*, 525–544. https://doi.org/10.1086/629606

Molnar, P. (2005). Mio-Pliocene growth of the Tibetan Plateau and evolution of East Asian Climate. *Palaeontologia Electronica*, *8*.

Najman, Y., Bickle, M., BouDagher-Fadel, M., Carter, A., Garzanti, E., Paul, M., et al. (2008). The Paleogene record of Himalayan erosion: Bengal Basin, Bangladesh. *Earth and Planetary Science Letters*, *273*(1–2), 1–14. https://doi.org/10.1016/j.epsl.2008.04.028

Najman, Y., Bickle, M., Garzanti, E., Pringle, M., Barfod, D., Brozovic, N., et al. (2009). Reconstructing the exhumation history of the Lesser Himalaya, NW India, from a multitechnique provenance study of the foreland basin Siwalik Group. *Tectonics*, *28*, 1–15. https://doi.org/10.1029/2009tc002506

Najman, Y., Bickle, M., Garzanti, E., Pringle, M., Barfod, D., Brozovic, N., et al. (2010). Correction to "Reconstructing the exhumation history of the Lesser Himalaya, NW India, from a multitechnique provenance study of the foreland basin Siwalik Group": CORRECTION. *Tectonics*, *29*(6). https://doi.org/10.1029/2010TC002778

Najman, Y., Sobel, E. R., Millar, I., Stockli, D. F., Govin, G., Lisker, F., et al. (2020). The exhumation of the Indo-Burman Ranges, Myanmar. *Earth and Planetary Science Letters*, *530*, 115948. https://doi.org/10.1016/j.epsl.2019.115948

Oliver, L., Harris, N., Bickle, M., Chapman, H., Dise, N., & Horstwood, M. (2003). Silicate weathering rates decoupled from the 87Sr/86Sr ratio of the dissolved load during Himalayan erosion. *Chemical Geology*, *201*, 119–139. https://doi.org/10.1016/s0009-2541(03)00236-5

Pickering, K. T., Carter, A., Andò, S., Garzanti, E., Limonta, M., Vezzoli, G., & Milliken, K. L. (2020). Deciphering relationships between the Nicobar and Bengal submarine fans, Indian Ocean. *Earth and Planetary Science Letters*, *544*, 116329. https://doi.org/10.1016/j.epsl.2020.116329

Quade, J., Cerling, T. E., & Bowman, J. R. (1989). Development of Asian monsoon revealed by marked ecological shift during the latest Miocene in northern Pakistan. *Nature*, *342*, 163–166. https://doi.org/10.1038/342163a0

Raymo, M. E. (1994). The Himalayas, organic carbon burial, and climate in the Miocene. *Paleoceanography*, *9*, 399–404. https://doi.org/10.1029/94pa00289

Raymo, M. E., & Ruddiman, W. F. (1992). Tectonic forcing of late Cenozoic climate. *Nature*, *359*, 117–122. https://doi.org/10.1038/359117a0

Retallack, G. J. (2001). Cenozoic expansion of grasslands and climatic cooling. *The Journal of Geology*, *109*, 407–426. https://doi.org/10.1086/320791

Richter, F. M., Rowley, D. B., & DePaolo, D. J. (1992). Sr isotope evolution of seawater: The role of tectonics. *Earth and Planetary Science Letters*, *109*, 11–23. https://doi.org/10.1016/0012-821x(92)90070-c

Robinson, R. A. J., Bird, M., Oo, N. W., Hoey, T., Aye, M. M., Higgitt, D., et al. (2007). The Irrawaddy river sediment flux to the Indian Ocean: The original nineteenth-century data revisited. *The Journal of Geology*, *115*, 629–640. https://doi.org/10.1086/521607

Singh, M., Singh, I. B., & Müller, G. (2007). Sediment characteristics and transportation dynamics of the Ganga River. *Geomorphology*, *86*, 144–175. https://doi.org/10.1016/j.geomorph.2006.08.011

Singh, S., Parkash, B., Awasthi, A., & Kumar, S. (2011). Late Miocene record of palaeovegetation from Siwalik palaeosols of the Ramnagar sub-basin, India. *Current Science*, 213–222.

Singh, S. K., & France-Lanord, C. (2002). Tracing the distribution of erosion in the Brahmaputra watershed from isotopic compositions of stream sediments. *Earth and Planetary Science Letters*, *202*, 645–662. https://doi.org/10.1016/s0012-821x(02)00822-1

Song, Z., Wan, S., Colin, C., Yu, Z., Révillon, S., Jin, H., et al. (2021). Paleoenvironmental evolution of South Asia and its link to Himalayan uplift and climatic change since the late Eocene. *Global and Planetary Change*, *200*, 103459. https://doi.org/10.1016/j.gloplacha.2021.103459

Srinivas, B., & Sarin, M. M. (2013). Atmospheric dry-deposition of mineral dust and anthropogenic trace metals to the Bay of Bengal. *Journal of Marine Systems*, *126*, 56–68. https://doi.org/10.1016/j.jmarsys.2012.11.004

Steinke, S., Groeneveld, J., Johnstone, H., & Rendle-Bühring, R. (2010). East Asian summer monsoon weakening after 7.5Ma: Evidence from combined planktonic foraminifera Mg/Ca and δ18O (ODP Site 1146; northern South China Sea). *Palaeogeography, Palaeoclimatology, Palaeoecology*, *289*, 33–43. https://doi.org/10.1016/j.palaeo.2010.02.007

Stoll, H. M., Vance, D., & Arevalos, A. (2007). Records of the Nd isotope composition of seawater from the Bay of Bengal: Implications for the impact of Northern Hemisphere cooling on ITCZ movement. *Earth and Planetary Science Letters*, *255*, 213–228. https://doi.org/10.1016/j.epsl.2006.12.016

Tanner, T., Hernández-Almeida, I., Drury, A. J., Guitián, J., & Stoll, H. (2020). Decreasing atmospheric CO_2 during the late Miocene cooling. *Paleoceanography and Paleoclimatology*, e2020PA003925.

Tauxe, L., & Feakins, S. J. (2020). A reassessment of the chronostratigraphy of late Miocene C3–C4 transitions. *Paleoceanography and Paleoclimatology*, *35*(7), e2020PA003857. https://doi.org/10.1029/2020pa003857

Tütken, T., Eisenhauer, A., Wiegand, B., & Hansen, B. T. (2002). Glacial-interglacial cycles in Sr and Nd isotopic composition of Arctic marine sediments triggered by the Svalbard/Barents Sea ice sheet. *Marine Geology*, *182*, 351–372. https://doi.org/10.1016/s0025-3227(01)00248-1

Unger, D., Ittekkot, V., Schäfer, P., Tiemann, J., & Reschke, S. (2003). Seasonality and interannual variability of particle fluxes to the deep Bay of Bengal: Influence of riverine input and oceanographic processes. *Deep Sea Research Part II: Topical Studies in Oceanography*, *50*, 897–923. https://doi.org/10.1016/s0967-0645(02)00612-4

Vannay, J.-C., Grasemann, B., Rahn, M., Frank, W., Carter, A., Baudraz, V., & Cosca, M. (2004). Miocene to Holocene exhumation of metamorphic crustal wedges in the NW Himalaya: Evidence for tectonic extrusion coupled to fluvial erosion. *Tectonics*, *23*, 1–24. https://doi.org/10.1029/2002tc001429

Vögeli, N., Najman, Y., van der Beek, P., Huyghe, P., Wynn, P. M., Govin, G., et al. (2017). Lateral variations in vegetation in the Himalaya since the Miocene and implications for climate evolution. *Earth and Planetary Science Letters*, *471*, 1–9. https://doi.org/10.1016/j.epsl.2017.04.037

Westerhold, T., Marwan, N., Drury, A. J., Liebrand, D., Agnini, C., Anagnostou, E., et al. (2020). An astronomically dated record of Earth's climate and its predictability over the last 66 million years. *Science*, *369*(6509), 1383. https://doi.org/10.1126/science.aba6853

Yang, Y., Ye, C., Galy, A., Fang, X., Xue, Y., Liu, Y., et al. (2020). Monsoon enhanced silicate weathering as a new atmospheric CO_2 consumption mechanism contributing to fast late Miocene global cooling. *Paleoceanography and Paleoclimatology*. e2020PA004008.

Zachos, J. C., Dickens, G. R., & Zeebe, R. E. (2008). An early Cenozoic perspective on greenhouse warming and carbon-cycle dynamics. *Nature*, *451*, 279–283. https://doi.org/10.1038/nature06588

References From the Supporting Information

Baker, J., Peate, D., Waight, T., & Meyzen, C. (2004). Pb isotopic analysis of standards and samples using a 207Pb–204Pb double spike and thallium to correct for mass bias with a double-focusing MC-ICP-MS. *Chemical Geology*, *211*, 275–303. https://doi.org/10.1016/j.chemgeo.2004.06.030

Bayon, G., Barrat, J. A., Etoubleau, J., Benoit, M., Bollinger, C., & Révillon, S. (2009). Determination of Rare Earth Elements, Sc, Y, Zr, Ba, Hf and Th in Geological Samples by ICP-MS after Tm Addition and Alkaline Fusion. *Geostandards and Geoanalytical Research*, *33*, 51–62. https://doi.org/10.1111/j.1751-908x.2008.00880.x

Belshaw, N., Freedman, P., O'Nions, R., Frank, M., & Guo, Y. (1998). A new variable dispersion double-focusing plasma mass spectrometer with performance illustrated for Pb isotopes. *International Journal of Mass Spectrometry*, *181*, 51–58. https://doi.org/10.1016/s1387-3806(98)14150-7

Cohen, A. S., O'Nions, R. K., Siegenthaler, R., & Griffin, W. L. (1988). Chronology of the pressure-temperature history recorded by a granulite terrain. *Contributions to Mineralogy and Petrology*, *98*, 303–311. https://doi.org/10.1007/bf00375181

Galer, S. J. G., & O'Nions, R. K. (1989). Chemical and isotopic studies of ultramafic inclusions from the San Carlos Volcanic Field, Arizona: A bearing on their Petrogenesis. *Journal of Petrology*, *30*, 1033–1064. https://doi.org/10.1093/petrology/30.4.1033

Jacobsen, S. B., & Wasserburg, G. J. (1980). Sm-Nd Isotopic Evolution of Chondrites. *Earth and Planetary Science Letters*, *50*, 139–155. https://doi.org/10.1016/0012-821x(80)90125-9

Jochum, K. P., Weis, U., Schwager, B., Stoll, B., Wilson, S. A., Haug, G. H., et al. (2016). Reference values following ISO guidelines for frequently requested rock reference materials. *Geostandards and Geoanalytical Research*, *40*, 333–350. https://doi.org/10.1111/j.1751-908x.2015.00392.x

Millot, R., Allègre, C.-J., Gaillardet, J., & Roy, S. (2004). Lead isotopic systematics of major river sediments: A new estimate of the Pb isotopic composition of the Upper Continental Crust. *Chemical Geology*, *203*, 75–90. https://doi.org/10.1016/j.chemgeo.2003.09.002

Pin, C., & Zalduegui, J. F. S. (1997). Sequential separation of light rare-earth elements, thorium and uranium by miniaturized extraction chromatography: Application to isotopic analyses of silicate rocks. *Analytica Chimica Acta*, *339*, 79–89. https://doi.org/10.1016/s0003-2670(96)00499-0

Steiger, R. H., & Jäger, E. (1977). Subcommission on Geochronology: Convention on the use of decay constants in geo- and cosmochronology. *Earth and Planetary Science Letters*, *36*, 359–362. https://doi.org/10.1016/0012-821x(77)90060-7

Tanaka, T., Togashi, S., Kamioka, H., Amakawa, H., Kagami, H., Hamamoto, T., et al. (2000). JNdi-1: A neodymium isotopic reference in consistency with LaJolla neodymium. *Chemical Geology*, *168*, 279–281. https://doi.org/10.1016/s0009-2541(00)00198-4

Vance, D., & Thirlwall, M. (2002). An assessment of mass discrimination in MC-ICPMS using Nd isotopes. *Chemical Geology*, *185*, 227–240. https://doi.org/10.1016/s0009-2541(01)00402-8

White, W. M., Albarède, F., & Télouk, P. (2000). High-precision analysis of Pb isotope ratios by multi-collector ICP-MS. *Chemical Geology*, *167*, 257–270. https://doi.org/10.1016/s0009-2541(99)00182-5